Ceramics International 47 (2021) 27462–27468

Contents lists available at ScienceDirect

Ceramics International

journal homepage: www.elsevier.com/locate/ceramint

The simulation for a high-efficiency millimeter wave microstrip antenna by low dielectric loss and wide temperature stable lithium-based microwave dielectric ceramics for LTCC applications

Yu Zhan, Lingxia Li *, Mingkun Du **

School of Microelectronics, Key Laboratory for Advanced Ceramics and Machining Technology of Ministry of Education, Tianjin Key Laboratory of Imaging and Sensing Microelectronic Technology, Tianjin University, Tianjin, 300072, China

ARTICLE INFO

Keywords:
Low sintering temperature
Low dielectric loss
Wide temperature stable
HFSS simulation
Millimeter wave microstrip antenna

ABSTRACT

As a common flux agent, B_2O_3–CuO was introduced into Li_2TiO_3 system to reduce the sintering temperature for the requirements of LTCC applications. The optimal mass ratio of CuO to B_2O_3 was innovatively explored. When the mass ratio of CuO to B_2O_3 increased to 1.2:1.0, excellent microwave dielectric properties were obtained in LTMF&LTZN$_{0.892}$+CB$_{1.2}$ ceramic of ε_r = 13.23, Q × f = 62,749 GHz, τ_f = -2.48 ppm/°C and the sintering temperature was reduced from 1300 to 930 °C. In a wide temperature range, the sample still maintain high temperature stability of $|\tau_f|$ < 5 ppm/°C (-40–120 °C). Based on the LTMF&LTZN$_{0.892}$+CB$_{1.2}$ substrate, a millimeter wave microstrip antenna resonated at 30.12 GHz was designed with a considerably high radiation efficiency of 93.94% and a signal gain of 4.87 dB. Comprehensive microwave dielectric properties make LTMF&LTZN$_{0.892}$+CB$_{1.2}$ become a candidate material for LTCC applications.

1. Introduction

As an advanced technology for passive integration and hybrid circuit packaging, LTCC technology (Low Temperature Co-fired Ceramic) can realize the overall firing of the laminated system through substrate interconnection and hot pressing of embedded components. Compared with traditional technology of device packaging, LTCC has many advantages. For example: (1) Low overall loss of system due to the low resistivity of metal electrode materials. (2) Good consistency and high reliability of the developed devices. (3) The high-density assembly of circuits and the miniaturization of devices are realized due to the multilayer interconnection structure, etc. At present, LTCC technology has gradually become the mainstream technology of passive integration, which is widely used in many fields such as communications and aerospace [1–4].

The performance of LTCC devices greatly depends on the properties of the materials, which should meet the following requirements: (1) In order to prevent the electrode materials (Au, Ag, Cu) from melting during the sintering process, the dielectric material needs to have a low sintering temperature (≤ 950 °C) (2) To reduce the overall loss of circuit, high Q × f value is required for the dielectric material (3) Excellent thermal stability is required to ensure the good matching and co-sintering of each part during the sintering process [5–7]. In addition, considering the requirement of high-speed device for time delay of signal transmission, low dielectric constant is necessary for the dielectric substrate as well [8,9].

In past few years, many researches on LTCC materials were carried out. Particularly, as a material without sintering agent, Mo-based LTCC ceramics exhibited excellent microwave dielectric properties. For example, Shi et al. prepared high-performance $Ce_2Zr_3(Mo_{0.9}W_{0.1}O_4)_9$ ceramics at 825 °C: ε_r = 9.85, Q × f = 22,980 GHz and a satisfactory τ_f value of -1.5 ppm/°C, which is suitable for LTCC applications in microwave devices [10]. With the development of lithium-based materials, Li_2TiO_3 has attracted great attention due to its good microwave dielectric properties: ε_r = 22.14, Q × f = 63,525 GHz, τ_f = 20.3 ppm/°C, ρ ~3.1 g/cm^3 [11]. However, the sintering temperature of Li_2TiO_3 system (~1300 °C) needs to be further reduced. In the past few decades, many researches of Li_2TiO_3 system for LTCC application have been carried out. For example, Zhang et al. prepared $Li_2Ti_{0.85}(Al_{0.5}Nb_{0.5})_{0.15}O_3$ + 1.5mol% $BaCu(B_2O_5)$: ε_r = 20.4, Q × f = 53,290 GHz, τ_f = 3.6 ppm/°C [12]. However, the dielectric loss needs to be improved. Hao et al. prepared Li_2TiO_3+2.5 wt% LiF: ε_r = 24.01, Q × f

* Corresponding author.
** Corresponding author.
E-mail addresses: Li_ling_xia_tju@163.com (L. Li), dmkun@tju.edu.cn (M. Du).

https://doi.org/10.1016/j.ceramint.2021.06.169
Received 26 April 2021; Received in revised form 17 June 2021; Accepted 21 June 2021
Available online 23 June 2021

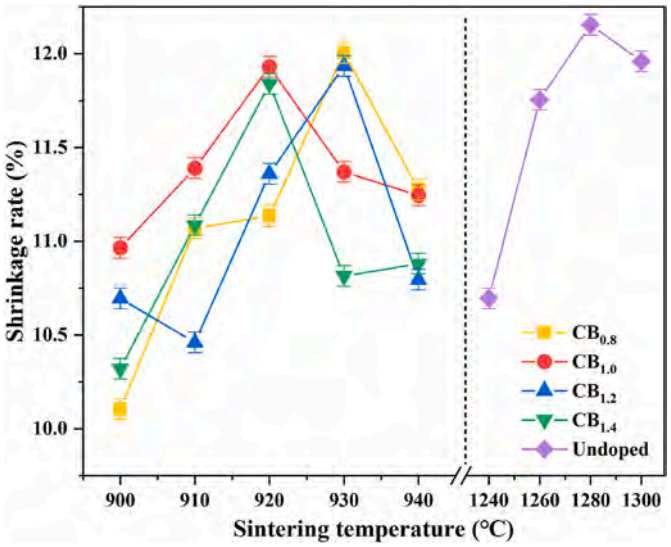

Fig. 1. The shrinkage rate of LTMF&LTZN$_{0.892}$+CB$_x$ ceramics sintered from 900 to 940 °C and undoped LTMF&LTZN$_{0.892}$ ceramic sintered from 1240 to 1300 °C.

= 75,500 GHz, τ_f = 36.2 ppm/°C [13]. While the temperature coefficient of the system is still too large. In addition, excellent properties were obtained of ε_r = 21.0, Q × f = 51,940 GHz and τ_f = 1.4 ppm/°C in $Li_2Ti_{1-x}(Cu_{1/3}Nb_{2/3})_xO_3$ + 3 wt% H_3BO_3 ceramic, as it reported by Guo et al., and the ε_r value needs to be further reduced in order to lower the time delay of LTCC devices [14]. At the same time, considering the impact of environmental changes, especially the regional temperature differences on the performance of LTCC devices, good temperature stability in a wide range is of great significance to the normal performance of LTCC devices as well [15].

Generally speaking, the reduction of sintering temperature is mainly achieved by two methods: (1) Chemical processing of highly active nano-scale powders [16]. (2) Adding low melting point flux agent [17,18]. Compared with the preparation of nano-scale powders, adding flux agent is considered as an economical and effective method. As a common flux agent, CuO–B_2O_3 can be used to reduce the sintering temperature of many kinds of materials [19,20]. In previous research of our group, 0.892 (Li_2TiO_3–2wt%MgF_2) + 0.108 $Li_2Mg_3Ti_{0.92}(Zn_{1/3}Nb_{2/3})_{0.08}O_6$ (abbreviated as LTMF&LTZN$_{0.892}$) ceramic was prepared at 1280 °C with excellent performance of ε_r = 17.98, Q × f = 145,916 GHz, τ_f = 0.19 ppm/°C. Therefore, 1 wt% (CuO–B_2O_3) was mixed into LTMF&LTZN$_{0.892}$ to reduce the sintering temperature of system for LTCC applications and the optimum mass ratio of CuO to B_2O_3 was then explored by means of the analysis of XRD patterns, Raman spectra, SEM micrographs and microwave dielectric properties of samples.

As the most precious resource in wireless communication system, the band, especially that in low frequency, has been unable to satisfy the requirements for massive data transmission. Therefore, higher frequency band like millimeter wave has gradually become one of the most important directions of 5G development [21,22]. As the core component of the wireless communication system, the function of the antenna is to transmit or receive electromagnetic waves. Therefore, the quality of communication system will be directly determined by the performance of antenna. Compared with traditional antennas, microstrip antennas have become the mainstream of current wireless communication system applications due to the advantages of small size, low cost and easy integration, which is mainly composed of dielectric substrate and microstrip line pattern [23]. In order to further explore the practical application value of the developed LTMF&LTZN$_{0.892}$+CB$_x$ ceramic, a high efficiency millimeter wave microstrip antenna was designed and stimulated using HFSS software based on the LTMF&LTZN$_{0.892}$+CB$_x$ dielectric substrate prepared in this work.

2. Experimental procedure

According to the stoichiometric ratio of Li_2TiO_3 and $Li_2Mg_3Ti_{0.92}(Zn_{1/3}Nb_{2/3})_{0.08}O_6$ (LMTZN), high-purity raw materials of Li_2CO_3 (98%, Yuan Li), MgO (98%, Comeo Chemical Reagent), TiO_2 (99%, Peng Da), ZnO (99.95%, Yuan Li) and Nb_2O_5 (99.99%, Jiu Jiang) were weighted and ball-milled in anhydrous ethanol for 12h. After drying, the powders of Li_2TiO_3 and LMTZN were calcined at 800 °C and 1000 °C for 4h, respectively. Subsequently, according to the stoichiometric ratio of [0.892 (Li_2TiO_3–2wt%MgF_2 (molar ratio is 0.966:0.034)) + 0.108 $Li_2Mg_3Ti_{0.92}(Zn_{1/3}Nb_{2/3})_{0.08}O_6$]+ 1 wt% (xCuO-$B_2O_3$) (abbreviated as LTMF&LTZN$_{0.892}$+CB$_x$ hereinafter), MgF_2 (99.99%) and xCuO–B_2O_3 (CuO, 99%, Yuan Li; B_2O_3, 98%, Tian Jiang; weight ratio of CuO to B_2O_3 was 0.8:1.0, 1.0:1.0, 1.2:1.0, 1.4:1.0, abbreviated as CB$_{0.8}$, CB$_{1.0}$, CB$_{1.2}$, CB$_{1.4}$ hereinafter) were added to the pre-sintering powders and the mixtures were re-grounded for 12h. After drying, the granulated powders were pressed into cylinder with 5 wt% paraffin mixed as binder and the green disks were prepared by uniaxial pressing under the pressure of 100Mpa. After expelling paraffin at 550 °C, all the cylinders were sintered at 900–940 °C for 4h raising from 550 °C at a rate of 5 °C/min to obtain compact ceramic structure.

X-ray powder diffraction (Rigaku, D/MAX-2500) was used to analyze the phase composition of samples. Raman spectrometer (Thermo Fisher, DXR Microscope) was used to record the Raman spectra. According to method of Archimedes, the apparent density (ρ_{mea}) was calculated. The scanning electron microscopy (Hitachi, Ltd., FE-SEM S-4800) was used to observe the surface morphology of samples. The network analyzer (Agilent, 8720 ES) was used to characterize the microwave dielectric

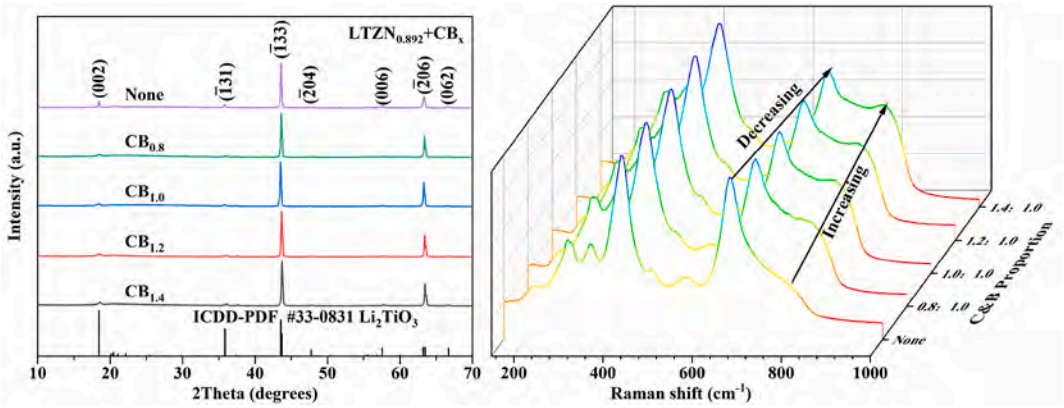

Fig. 2. (a) XRD pattern and (b) Raman spectra of LTMF&LTZN$_{0.892}$ and LTMF&LTZN$_{0.892}$+CB$_x$ ceramics sintered at optimum temperature.

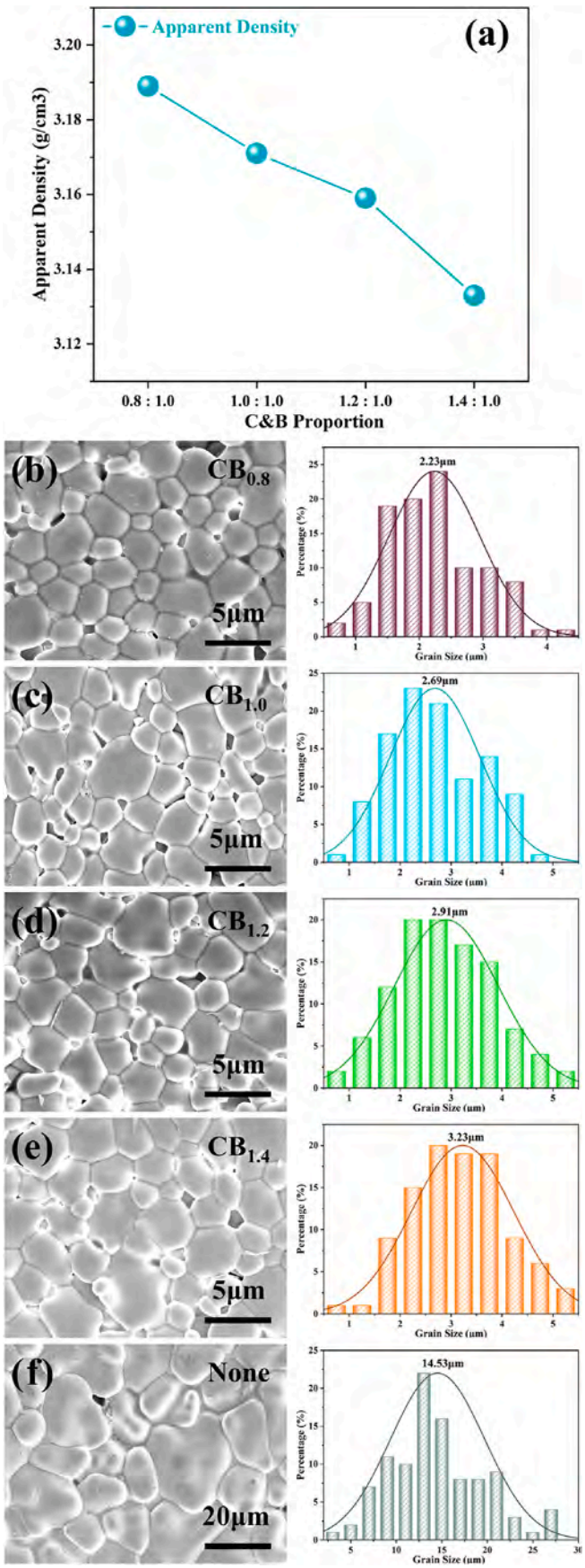

Fig. 3. (a) Variation of bulk density (b–e) The SEM images and grain distribution of LTMF&LTZN$_{0.892}$+CB$_x$ ceramics sintered at optimum temperature.

properties. Among them, TE_{011} resonant mode was used to test the permittivity according to the Hakki-Coleman method [24] and $TE_{01\delta}$ mode was used to test the $Q \times f$ values by cavity method [25]. The τ_f values can be measured as follows:

$$\tau_f = \frac{f_{T_1} - f_{T_2}}{f_{T_2}(T_1 - T_2)} \times 10^6 \ (ppm/^\circ C) \tag{1}$$

In above formula, f_{T_1} and f_{T_2} denote the resonant frequency at T_1 and T_2, which were measured by placing the ceramics into two kinds of temperature chamber, including a low temperature chamber (GZ-ESPEC GMC-71) and a high-temperature chamber (GZ-ESPEC STH-120) used at -40–120 °C and 25–85 °C, respectively, and then tested at a series of temperature points.

Before carrying out the simulation, the initial parameters of the antenna can be estimated. The width of the rectangular patch (W) can be calculated as follows [26]:

$$W = \frac{c}{2f_0}\left(\frac{\varepsilon_r + 1}{2}\right)^{\frac{1}{2}} \tag{2}$$

In above formula, c is the light speed. f_0 is the center frequency. The length of the patch is approximately half of the mid-wavelength. Due to the edge effect of the radiation patch, the radiation gap should be taken into account and the length of the patch (L) should be corrected as follows [27]:

$$L = \frac{c}{2f_0\sqrt{\varepsilon_e}\sqrt{\mu_0\varepsilon_0}} - 2\Delta L \tag{3}$$

In above formula, ε_0 and μ_0 represent the permittivity and permeability in free space, respectively. In addition, ΔL and ε_e represent the equivalent radiation gap width and the effective dielectric constant respectively, which are defined by the following equations [28,29]:

$$\Delta L = 0.412h\frac{(\varepsilon_e + 0.3)(W/h + 0.264)}{(\varepsilon_e - 0.258)(W/h + 0.8)} \tag{4}$$

$$\varepsilon_e = \frac{\varepsilon_r + 1}{2} + \frac{\varepsilon_r - 1}{2}\left(1 + \frac{12h}{W}\right)^{\frac{1}{2}} \tag{5}$$

Where h represents the substrate thickness. It is necessary to add a wavelength impedance converter in front of the microstrip line in order to match the edge impedance of the microstrip antenna and make it conform to the 50 Ω system which is commonly used by microwave devices. The conditions of impedance matching can be expressed as follows:

$$Z_1 = \sqrt{Z_0 Z_L} \tag{6}$$

Where Z_1 is characteristic impedance of wavelength impedance converter, Z_0 is characteristic impedance of microstrip line, and Z_L is the edge impedance of the antenna. The optimization of antenna physical parameters is carried out by HFSS software.

3. Results and discussion

Fig. 1 presents the shrinkage rate of LTMF&LTZN$_{0.892}$+CB$_x$ ceramics sintered from 900 to 940 °C and undoped LTMF&LTZN$_{0.892}$ ceramic sintered from 1240 to 1300 °C. For undoped LTMF&LTZN$_{0.892}$, the maximum shrinkage rate was obtained at 1280 °C. After doping, the sintering temperature corresponding to the maximum shrinkage rate is obviously reduced. For LTMF&LTZN$_{0.892}$+CB$_{0.8}$ and LTMF&LTZN$_{0.892}$+CB$_{1.0}$, the maximum appeared at 920 °C and for the other two proportion, the maximum appeared at 930 °C. It proves that the sintering temperature of the system was effectively reduce to below 950 °C by the CB additive, meeting the requirements of the LTCC technology.

In order to explore the effect of CB additive on phase composition,

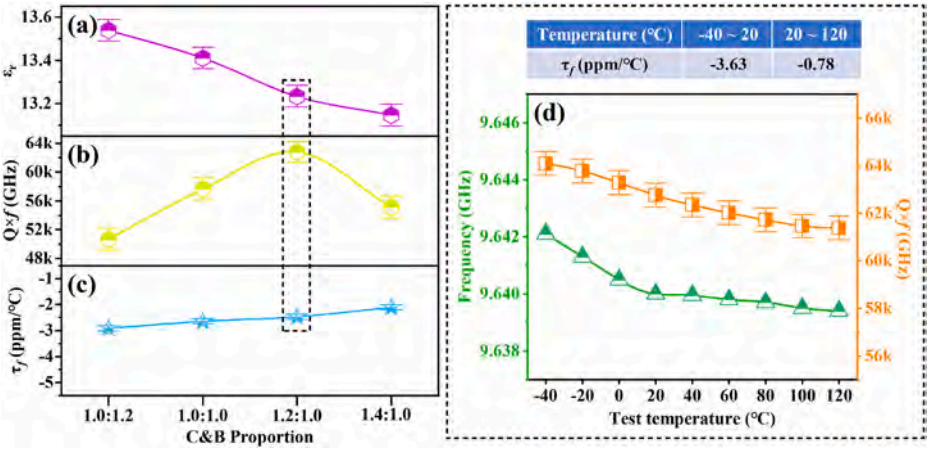

Fig. 4. (a–c) The variation of microwave dielectric properties as a function of C&B proportion at optimum temperature. (e) Variation of Q × *f* values and resonant frequencies in wide temperature range of LTMF&LTZN$_{0.892}$+CB$_{1.2}$ ceramic sintered at 930 °C.

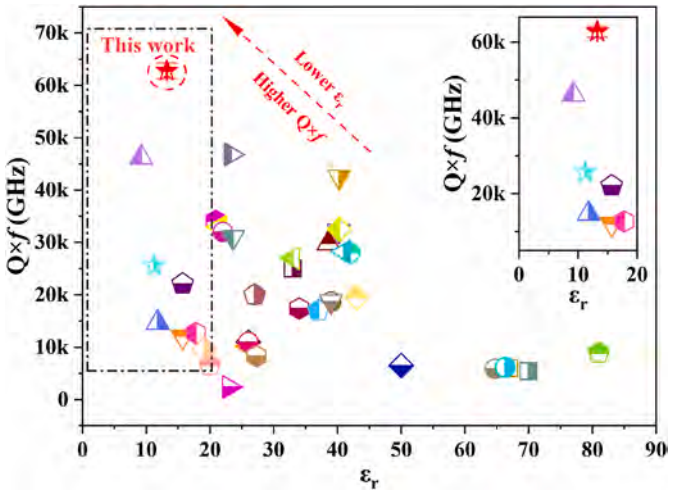

Fig. 5. The statistical diagram of ε_r values and Q × *f* values of near-zero temperature coefficient ($|\tau_f| < 10$ ppm/°C) and low sintering temperature (S. T. ≤ 950 °C) microwave dielectric ceramics.

the X-ray diffraction patterns of undoped LTMF&LTZN$_{0.892}$ and LTMF&LTZN$_{0.892}$+CB$_x$ ceramics sintered at optimum temperature was characterized in Fig. 2(a). Indexed from the standard PDF-card of Li_2TiO_3 (ICDD-PDF #33-0831), all diffraction peaks can be found and no second phase was observed, which indicates that the CB flux agent did not crystallize, but existed in the crystal lattice in an amorphous state. The same phenomenon has been reported in previous studies [30,31]. In order to explore the variation in crystal structure, the Raman spectroscopy was characterized, as shown in Fig. 2(b). All spectra exhibit the similar Raman active vibration modes to those of monoclinic Li_2TiO_3 as it reported previously. According to group theory, the Raman vibration modes at 550-700 cm^{-1} mainly contribute to the stretch of Ti-O bond in [TiO_6] octahedra, and that at 250-400 cm^{-1} mainly contribute to the bend of O-Li-O and the stretch of Li-O bond in [LiO_6] octahedra [12,32]. With the increase of CuO ratio, the intensity of characteristic peaks slightly decreased, which reflects the decline of cation ordering [33]. In addition, the intensity of the characteristic peak located at 800 cm^{-1} gradually increased, which can be explained by the relaxations of selection rules caused by the reduce of crystal symmetry at the short-range ordering domain boundaries [12,34]. Namely, the mass ratio of CB has no effect on the phase of the system, but can slightly affect the crystal structure.

Fig. 3(a) exhibits the bulk densities of LTMF&LTZN$_{0.892}$+CB$_x$ ceramics as a function of C&B proportion. With the increase of CuO ratio, the bulk densities of samples gradually decreased. Fig. 3(b–e) presents the SEM micrographs of LTMF&LTZN$_{0.892}$+CB$_x$ ceramic. As shown in figure, all samples exhibit dense and fine microstructure. Small amounts of pores exist on the surface, which may be caused by the volatilization of Li element. Fig. 3(f) presents the SEM micrographs of LTMF&LTZN$_{0.892}$ ceramic. For more specific characterization of the variation of grain size, the grain distribution is counted by means of ImageJ software, as embedded in SEM images. It can be calculated that the average grain size of LTMF&LTZN$_{0.892}$ ceramic is 14.53 μm, and that of LTMF&LTZN$_{0.892}$+CB$_x$ fluctuated in the range of 2–4 μm, which is far less than undoped sample. This is mainly because during the high-temperature sintering process, the liquid phase produced from CuO-B_2O_3 will promote the occurrence of crystallization and molecular arrangement, and accelerate the sintering process of samples based on liquid phase transport, which is also the essence of reducing the sintering temperature of the system [30,35,36]. In addition, with the increase of CuO, the grain size of the sample gradually increased. For CuO-B_2O_3, higher ratio of CuO will suppress the production of liquid phase, resulting in higher surface energy and eventually promote grain growth, which is consistent with the variation of average grain size. At the same time, the liquid phase transport will promote the discharge of gas in the gap as well, which also explains the variation trend of the density.

Fig. 4(a) presents the variation of microwave dielectric properties sintered at optimum temperature as a function of C&B proportion. With the increase of CuO ratio, the ε_r values decreased linearly, exhibiting the same trend with density, which indicated that the density may be the key factor affecting the ε_r values. Fig. 4(b) present the Q × *f* values of samples. With the increase of mass ratio of CuO, the Q × *f* values firstly increased, and the maximum was obtained of 62,749 GHz for LTMF&LTZN$_{0.892}$+CB$_{1.2}$. As discussed in SEM, the increase of CuO ratio will greatly inhibit the formation of the liquid phase and promote the grain growth, resulting in an increasing trend in grain size and a decreasing trend in grain boundaries. As we all know, the grain boundaries, which act as the two-dimensional defects in the structure, will interrupt the perfect symmetry of the crystal, eventually leading to the increase of lattice loss. As the mass ratio of CuO further increased, the Q × *f* values tended to decrease. It can be speculated that the porosity has become the main factor determining the dielectric loss because of the decrease of grain boundaries content. Fig. 4(c) presents the variation of τ_f values, which gradually increased towards near-zero. However, the magnitude of the change is relatively small, remaining close to zero, which indicates that the temperature coefficient is not sensitive to the ratio of CB. As a key parameter used to evaluate the temperature stability of the devices, τ_f values were measured at

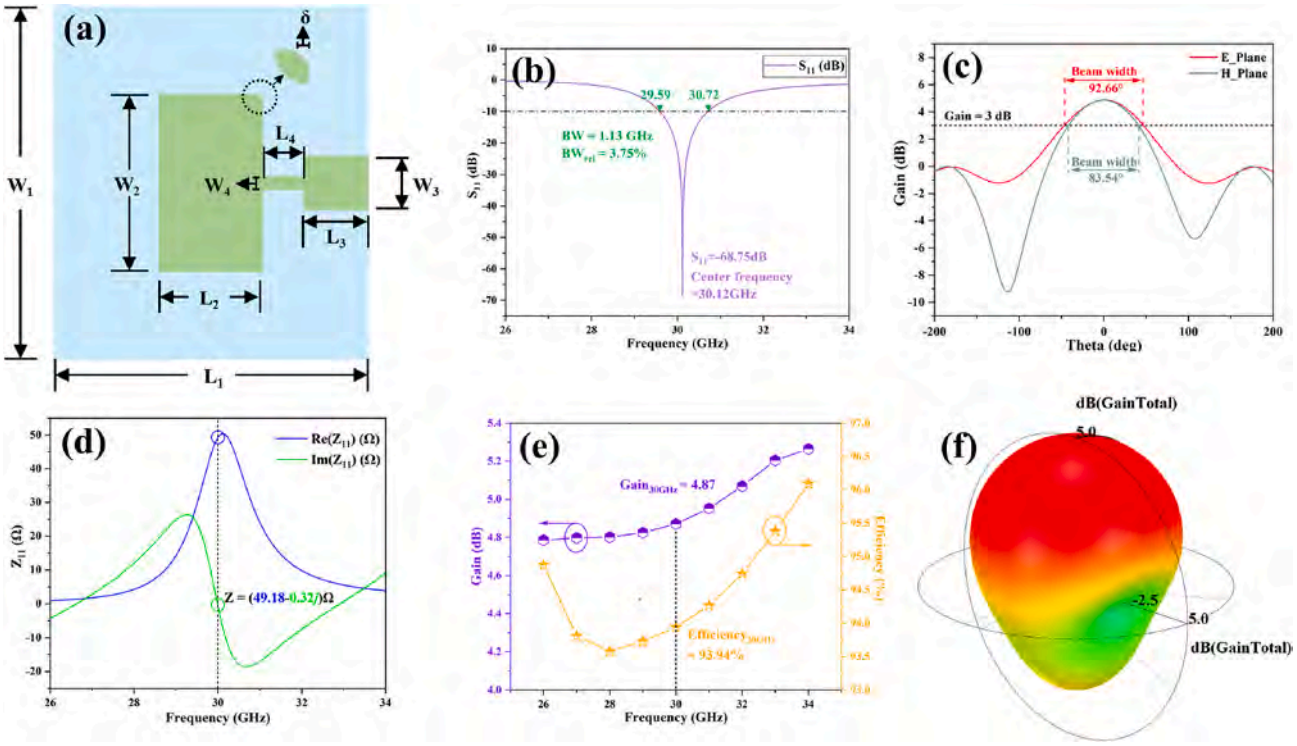

Fig. 6. (a) The geometry of antenna. The simulation of (b) S_{11} result (c) radiation pattern of E plane and H plane (d) transmission impedance (e) gains and radiation efficiencies as a function of frequency (f) 3D radiation pattern.

Table 1
The optimum parameters of the simulated antenna.

Parameters	W_1	W_2	W_3	W_4	L_1	L_2	L_3	L_4	δ	h
Values (mm)	3.86	1.93	0.6	0.2	3.58	1.18	0.7	0.5	0.05	0.4

25–85 °C most of time [37–39]. In order to explore the wide temperature stability of samples, the test temperature was extended to -40–120 °C, as shown in Fig. 4(d). With the increase of test temperature, the resonant frequency of samples firstly decreased, and then tended to be stable. Therefore, there are two τ_f values of samples in a wide temperature range, which was equal to -3.63 ppm/°C and -0.78 ppm/°C in the range of -40–20 °C and 20–120 °C, respectively, remaining near zero. At the same time, the $Q \times f$ values were also measured in a wide range and exhibited a slightly declining trend, which can be explained by the intensification of lattice vibration. Macroscopically, the $Q \times f$ values of the sample fluctuates slightly. All the above results show that the sample has good temperature stability in a wide range.

In order to compare the performance of LTMF&LTZN$_{0.892}$+CB$_{1.2}$ with other system suitable for LTCC application, some materials with low sintering temperature (S.T. ≤ 950 °C) and near-zero τ_f value ($|\tau_f| <$ 10 ppm/°C) were selected here from the book of Sebastian [40]. As shown in Fig. 5, compared with other systems with low dielectric constant ($\varepsilon_r < 20$), LTMF&LTZN$_{0.892}$+CB$_{1.2}$ prepared in this work has the higher $Q \times f$ value, which will be conducive to the improvement of antenna efficiency. At the same time, its wide temperature stability can ensure the antenna works normally in different environments. In a word, comprehensive and excellent microwave dielectric properties make LTMF&LTZN$_{0.892}$+CB$_{1.2}$ become a preferred candidate material for LTCC application.

In order to quantitatively analyze the contribution of the excellent dielectric properties of LTMF&LTZN$_{0.892}$+CB$_{1.2}$ in the performance of LTCC devices, based on LTMF&LTZN$_{0.892}$+CB$_{1.2}$ substrate, a millimeter wave microstrip antenna was designed for the center frequency of 30 GHz. Microstrip antennas have a variety of feeding methods. Among them, the microstrip line feeding is considered as one of the most commonly used methods, which mainly realizes power feeding through the microstrip transmission line integrated with the microstrip radiation patch [41,42]. Therefore, this design applied the microstrip line feed mode, where the feeder and the patch unit were set to be coplanar, and used the wave port side feed mode to feed the center of the wide side of the rectangular patch. The input impedance of transmission line is 50Ω. Based on the initial calculated physical size of the microstrip antenna, the optimal solution can be obtained by means of "Optimetrics" module in HFSS. In the optimization stage, the patch size is finetuned to achieve the matching of edge impedance. On this basis, a wavelength impedance converter is set for the transmission line to match the input impedance with the patch edge impedance, so as to obtain the maximum transmission power. At the same time, corner cutting can be used to reduce the impact of discontinuity at the corners of the patch on the transmission.

Fig. 6(a) presents the geometry of the designed millimeter wave microstrip antenna and the optimized parameters are listed in Table 1. According to the simulated S_{11} result, as shown in Fig. 6(b), the resonant frequency of the antenna is 30.12 GHz, which belongs to the millimeter wave frequency. The frequency range that satisfies $S_{11} <$ -10 dB is 29.59–30.72 GHz. Therefore, the effective working bandwidth of the antenna is 1.13 GHz, with a relative bandwidth of 3.75%. In addition, the S_{11} result at the resonance point is as low as -68.75 dB, which indicates that the antenna unit has a small reflected wave loss at the resonance point. Fig. 6(c) exhibits the impedance simulation results, which is equal to $Z = (49.18–0.32j)\ \Omega$, at the resonance frequency. It proves that the antenna impedance is well matched. Fig. 6(d) presents the simulated radiation pattern of H plane and E plane. As shown in

figure, the beam width for H plane and E plane is 83.54° and 92.66°, respectively, exhibiting a wide radiation angle. Fig. 6(e) exhibits the simulated antenna signal gains and radiation efficiencies as a function of frequency. Excellent signal gain of 4.87 dB and a considerable high radiation efficiency of 93.94% were obtained at the center frequency, and slightly fluctuates with the variation of frequency. In addition, it can be seen from the simulated 3D radiation pattern shown in Fig. 6(f) that the antenna has good radiation symmetry. However, for the single antenna, there are still some problems. For example, the working frequency band of antenna is still narrow. In addition, the lobe width is wide, resulting in the dispersion of the radiation energy. And the signal gain needs to be further increased. These problems can be solved by the design of microstrip antenna array, which will be further developed in the follow-up research.

4. Conclusion

In this work, CuO–B_2O_3 was introduced into Li_2TiO_3 system for LTCC applications. According to XRD and Raman results, the doped CB was not crystallized, but existed in amorphous state. In addition, the doped CB has no effect on the phase of the system, but can slightly affect the crystal structure. With the increase of CuO ratio, the grain size tended to increase due to the effect of liquid phase transport. When the mass ratio of CuO to B_2O_3 increased to 1.2:1.0, excellent microwave dielectric properties was obtained in LTMF&LTZN$_{0.892}$+CB$_{1.2}$: $\varepsilon_r = 13.23$, $Q \times f =$ 62,749 GHz, $\tau_f =$ -2.48 ppm/°C. In a wide temperature range, the sample still maintain high temperature stability of $|\tau_f| < 5$ ppm/°C (-40 to 120 °C). Based on the above materials, a considerably high radiation efficiency of 93.94% can be obtained on the designed millimeter wave microstrip antenna resonated at 30.12 GHz with a signal gain of 4.87 dB and a bandwidth of 1.13 GHz. Comprehensive microwave dielectric properties make it become an ideal candidate for LTCC application.

Declaration of competing interest

The authors declare that they have no known competing financial interests or personal relationships that could have appeared to influence the work reported in this paper.

Acknowledgements

This work was supported by the National Key R&D Program of China (Grant no. 2017YFB0406300). The authors thank Mr Jianli Qiao for his help in using Raman spectrometer (Thermo Fisher, DXR Microscope).

References

[1] H.Z. Zuo, X.L. Tang, H. Guo, Q.G. Wang, C.L. Dai, H.W. Zhang, H. Su, Effects of BaCu(B_2O_5) addition on microwave dielectric properties of Li_2TiO_3 ceramics for LTCC applications, Ceram. Int. 43 (2017) 13913–13917, https://doi.org/10.1016/j.ceramint.2017.07.119.

[2] J.X. Bi, Y.J. Niu, H.T. Wu, $Li_4Mg_3Ti_2O_9$: a novel low-loss microwave dielectric ceramic for LTCC applications, Ceram. Int. 43 (2017) 7522–7530, https://doi.org/10.1016/j.ceramint.2017.03.041.

[3] D.K. Kwon, M.T. Lanagan, T.R. Shrout, Microwave dielectric properties and low-temperature cofiring of $BaTe_4O_9$ with aluminum metal electrode, J. Am. Ceram. Soc. 88 (2005) 3419–3422, https://doi.org/10.1111/j.1551-2916.2005.00613.x.

[4] S.H. Lei, H.Q. Fan, W.N. Chen, Z.Y. Liu, M.M. Li, Structure, microwave dielectric properties, and novel low-temperature sintering of $xSrTiO_3$–$(1-x)LaAlO_3$ ceramics with LTCC application, J. Am. Ceram. Soc. 100 (2017) 235–246, https://doi.org/10.1111/jace.14548.

[5] M.T. Sebastian, H. Jantunen, Low loss dielectric materials for LTCC applications: a review, Int. Mater. Rev. 53 (2008) 57–90, https://doi.org/10.1179/174328008X277524.

[6] M.F. Zhong, H. Su, X.L. Jing, Y.X. Li, Q.H. Lu, Y.L. Jing, Crystal structure and microwave dielectric properties of $Li_2Mg_{0.6-x}Co_xZn_{0.4}SiO_4$ ceramic for LTCC applications, Ceram. Int. 46 (2020) 13095–13101, https://doi.org/10.1016/j.ceramint.2020.02.081.

[7] H.L. Pan, Y.X. Mao, L. Cheng, H.T. Wu, New $Li_3Ni_2NbO_6$ microwave dielectric ceramics with the orthorhombic structure for LTCC applications, J. Alloys Compd. 723 (2017) 667–674, https://doi.org/10.1016/j.jallcom.2017.06.285.

[8] M. Xiao, Y.S. Wei, P. Zhang, The effect of sintering temperature on the crystal structure and microwave dielectric properties of $CaCoSi_2O_6$ ceramic, Mater. Chem. Phys. 225 (2019) 99–104, https://doi.org/10.1016/j.matchemphys.2018.12.027.

[9] H. Ohsato, J. Varghese, A. Kan, J.S. Kim, I. Kagomiya, H. Ogawa, M.T. Sebastian, H. Jantunen, Volume crystallization and microwave dielectric properties of indialite/cordierite glass by TiO_2 addition, Ceram. Int. 47 (2021) 2735–2742, https://doi.org/10.1016/j.ceramint.2020.09.126.

[10] L. Shi, C. Liu, H.W. Zhang, Effects of W^{6+} substitution on the microwave dielectric properties of $Ce_2Zr_3(MoO_4)_9$ ceramics, J. Adv. Dielect. 9 (2019) 1950049, https://doi.org/10.1142/S2010135X19500498.

[11] L.L. Yuan, J.J. Bian, Microwave dielectric properties of the lithium containing compounds with rock salt structure, Ferroelectrics 387 (2009) 123–129, https://doi.org/10.1080/00150190902966610.

[12] T.W. Zhang, R.Z. Zuo, J. Zhang, Structure, Microwave dielectric properties, and low-temperature sintering of acceptor/donor codoped $Li_2Ti_{1-x}(Al_{0.5}Nb_{0.5})_xO_3$ Ceramics, J. Am. Ceram. Soc. 99 (2016) 825–832, https://doi.org/10.1111/jace.14055.

[13] Y.Z. Hao, H. Yang, G.H. Chen, Q.L. Zhang, Microwave dielectric properties of Li_2TiO_3 ceramics doped with LiF for LTCC applications, J. Alloys Compd. 552 (2013) 173–179, https://doi.org/10.1016/j.jallcom.2012.10.110.

[14] H.H. Guo, M.S. Fu, D. Zhou, C. Du, P.J. Wang, L.X. Pang, W.F. Liu, A.S.B. Sombra, J.Z. Su, Design of a high-efficiency and -gain antenna using novel low-loss, temperature-stable $Li_2Ti_{1-x}(Cu_{1/3}Nb_{2/3})_xO_3$ microwave dielectric ceramics, ACS Appl. Mater. Interfaces 13 (2021) 912–923, https://doi.org/10.1021/acsami.0c18836.

[15] L.Z. Ni, L.X. Li, M.K. Du, Ultra-high-Q and wide temperature stable $Ba(Mg_{1/3}Ta)O_3$ microwave dielectric ceramic for 5G-oriented dielectric duplexer adhibition, J. Alloys Compd. 844 (2020) 156106, https://doi.org/10.1016/j.jallcom.2020.156106.

[16] M.J. Wu, Y.C. Zhang, J.D. Chen, M.Q. Xiang, Microwave dielectric properties of sol-gel derived $NiZrNb_2O_8$ ceramics, J. Alloys Compd. 747 (2018) 394–400, https://doi.org/10.1016/j.jallcom.2018.02.300.

[17] Y. Zhang, Y.C. Zhang, M.Q. Xiang, S.Y. Liu, H. Liu, Low temperature sintering and microwave dielectric properties of $CoTiNb_2O_8$ ceramics with CuO addition, Ceram. Int. 42 (2016) 3542–3547, https://doi.org/10.1016/j.ceramint.2015.10.162.

[18] T. Takada, S.F. Wang, S. Yoshikawa, S.J. Jang, R.E. Newnham, Effects of glass additions on (Zr,Sn)TiO_4 for microwave applications, J. Am. Ceram. Soc. 77 (1994) 2485–2488, https://doi.org/10.1111/j.1151-2916.1994.tb04629.x.

[19] J.B. Lim, Y.H. Jeong, N.H. Nguyen, S. Nahm, J.H. Paik, J.H. Kim, H.J. Lee, Low temperature sintering of the $Ba_2Ti_9O_{20}$ ceramics using B_2O_3/CuO and BaCu(B_2O_5) additives, J. Eur. Ceram. Soc. 27 (2007) 2875–2879, https://doi.org/10.1016/j.jeurceramsoc.2006.11.043.

[20] D.K. Yim, J.R. Kim, D.W. Kim, K.S. Hong, Microwave dielectric properties and low-temperature sintering of $Ba_3Ti_4Nb_4O_{21}$ ceramics with B_2O_3 and CuO additions, J. Eur. Ceram. Soc. 27 (2007) 3053–3057, https://doi.org/10.1016/j.jeurceramsoc.2006.11.029.

[21] E. Hossain, M. Rasti, H. Tabassum, A. Abdelnasser, Evolution toward 5G multi-tier cellular wireless networks: an interference management perspective, IEEE Wirel. Commun. 21 (2014) 118–127, https://doi.org/10.1109/MWC.2014.6845056.

[22] J.G. Andrews, S. Buzzi, W. Choi, S.V. Hanly, A. Lozano, A.C.K. Soong, J.C. Zhang, What will 5G be? IEEE J. Sel. Area. Commun. 32 (2014) 1065–1082, https://doi.org/10.1109/JSAC.2014.2328098.

[23] M. Weiss, Microstrip antennas for millimeter waves, IEEE Trans. Antenn. Propag. 29 (1981) 171–174, https://doi.org/10.1109/TAP.1981.1142547.

[24] B.W. Hakki, P.D. Coleman, A dielectric resonator method of measuring inductive capacities in the millimeter range, IEEE Trans. Microw. Theor. Tech. 8 (1960) 402–410, https://doi.org/10.1109/TMTT.1960.1124749.

[25] W.E. Courtney, Analysis and evaluation of a method of measuring the complex permittivity and permeability microwave insulators, IEEE Trans. Microw. Theor. Tech. 18 (1970) 476–485, https://doi.org/10.1109/TMTT.1970.1127271.

[26] B. Garg, N. Agrawal, V. Sharma, A. Tomar, P. Dubey, Rectangular microstrip patch antenna with “pentagonal rings” shaped metamaterial cover, in: 2012 International Conference on Communication Systems and Network Technologies, 2012, pp. 40–44, https://doi.org/10.1109/CSNT.2012.18.

[27] J.D. Zhang, L. Zhu, Q.S. Wu, N.W. Liu, W. Wu, A compact microstrip-fed patch antenna with enhanced bandwidth and harmonic suppression, IEEE Trans. Antenn. Propag. 64 (2016) 5030–5037, https://doi.org/10.1109/TAP.2016.2618539.

[28] A.K. Sidhu, J.S. Sivia, Microstrip rectangular patch antenna for S and X band applications, in: 2016 International Conference on Wireless Communications, Signal Processing and Networking (WiSPNET), 2016, pp. 248–251, https://doi.org/10.1109/WiSPNET.2016.7566130.

[29] S. Feng, L. Zhang, H.W. Yu, Y.X. Zhang, Y.C. Jiao, A single-layer wideband differential-fed microstrip patch antenna with complementary split-ring resonators loaded, IEEE Access 7 (2019) 132041–132048, https://doi.org/10.1109/ACCESS.2019.2940279.

[30] L.X. Pang, D. Zhou, Microwave dielectric properties of low-firing Li_2MO_3 (M=Ti, Zr, Sn) ceramics with B_2O_3-CuO addition, J. Am. Ceram. Soc. 93 (2010) 3614–3617, https://doi.org/10.1111/j.1551-2916.2010.04152.x.

[31] H.H. Guo, D. Zhou, C. Du, P.J. Wang, W.F. Liu, L.X. Pang, Q.P. Wang, J.Z. Su, C. Singh, S. Trukhanov, Temperature stable $Li_2Ti_{0.75}(Mg_{1/3}Nb_{2/3})_{0.25}O_3$-based microwave dielectric ceramics with low sintering temperature and ultra-low dielectric loss for dielectric resonator antenna applications, J. Mater. Chem. C. 8 (2020) 4690–4700, https://doi.org/10.1039/D0TC00326C.

[32] H.H. Guo, D. Zhou, L.X. Pang, J.Z. Su, Influence of ($Mg_{1/3}Nb_{2/3}$) complex substitutions on crystal structures and microwave dielectric properties of Li_2TiO_3

ceramics with extreme low loss, J. Materiomics. 4 (2018) 368–382, https://doi.org/10.1016/j.jmat.2018.09.002.
[33] N.X. Xu, J.H. Zhou, H. Yang, Q.L. Zhang, M.J. Wang, L. Hu, Structural evolution and microwave dielectric properties of MgO–LiF co-doped Li_2TiO_3 ceramics for LTCC applications, Ceram. Int. 40 (2014) 15191–15198, https://doi.org/10.1016/j.ceramint.2014.06.134.
[34] Y.M. Ding, J.J. Bian, Structural evolution, sintering behavior and microwave dielectric properties of $(1-x)Li_2TiO_3+xLiF$ ceramics, Mater. Res. Bull. 48 (2013) 2776–2781, https://doi.org/10.1016/j.materresbull.2013.03.043.
[35] A.Y. Borisevich, P.K. Davies, Effect of V_2O_5 Doping on the sintering and dielectric properties of M-phase $Li_{1+x-y}Nb_{1-x-3y}Ti_{x+4y}O_3$ ceramics, J. Am. Ceram. Soc. 87 (2004) 1047–1052, https://doi.org/10.1111/j.1551-2916.2004.01047.x.
[36] J.H. Zhu, J.Y. Liu, Y. Zeng, Low temperature sintering and microwave dielectric properties of Li_2O–3ZnO–$5TiO_2$ ceramics doped with V_2O_5, J. Mater. Sci. Mater. Electron. 29 (2018) 14455–14461, https://doi.org/10.1007/s10854-018-9578-y.
[37] P. Zhang, H. Xie, Y.G. Zhao, M. Xiao, Microwave dielectric properties of low loss $Li_2(Mg_{0.95}A_{0.05})_3TiO_6$ ($A = Ca^{2+}$, Ni^{2+}, Zn^{2+}, Mn^{2+}) ceramics system, J. Alloys Compd. 689 (2016) 246–249, https://doi.org/10.1016/j.jallcom.2016.07.198.
[38] A. Ullah, H.X. Liu, H. Hao, J. Iqbal, Z.H. Yao, M.H. Cao, Influence of TiO_2 additive on sintering temperature and microwave dielectric properties of $Mg_{0.90}Ni_{0.1}SiO_3$ ceramics, J. Eur. Ceram. Soc. 37 (2017) 3045–3049, https://doi.org/10.1016/j.jeurceramsoc.2017.03.047.
[39] Z.P. Xu, L.X. Li, S.H. Yu, M.K. Du, W.J. Luo, Microstructure and microwave dielectric characteristics of magnesium fluoride additive to $MgTiO_3$-$(Ca_{0.8}Sr_{0.2})TiO_3$ ceramics, Mater. Lett. 252 (2019) 191–193, https://doi.org/10.1016/j.matlet.2019.05.136.
[40] M.T. Sebastian, Dielectric Materials for Wireless Communication, Elsevier Science, 2010.
[41] R. Mailloux, J. McIlvenna, N. Kernweis, Microstrip array technology, IEEE Trans. Antenn. Propag. 29 (1981) 25–37, https://doi.org/10.1109/TAP.1981.1142525.
[42] D.M. Pozar, Microstrip antennas, Proc. IEEE 80 (1992) 79–91, https://doi.org/10.1109/5.119568.